Lab on a Chip

View Online
Dynamic Article Links

Cite this: *Lab Chip*, 2011, **11**, 2460

www.rsc.org/loc

**TECHNICAL NOTE**

# Mesoporous silica as a membrane for ultra-thin implantable direct glucose fuel cells†

**Tushar Sharma,‡[a] Ye Hu,‡[b] Meryl Stoller,[c] Marc Feldman,[de] Rodney S. Ruoff,[c] Mauro Ferrari[b] and Xiaojing Zhang*[a]**

***Received 10th February 2011, Accepted 3rd May 2011***
**DOI: 10.1039/c1lc20119k**



The design, fabrication and characterization of an inorganic catalyst based direct glucose fuel cell using mesoporous silica coating as a functional membrane is reported. The desired use of mesoporous silica based direct glucose fuel cell is for a blood vessel implantable device. Blood vessel implantable direct glucose fuel cells have access to higher continuous glucose concentrations. However, reduction in the implant thickness is required for application in the venous system as part of a stent. We report development of an implantable device with a platinum thin-film (thickness: 25 nm) deposited on silicon substrate (500 μm) to serve as the anode, and graphene pressed on a stainless steel mesh (175 μm) to serve as the cathode. Control experiments involved the use of a surfactant-coated polypropylene membrane (50 μm) with activated carbon (198 μm) electrodes. We demonstrate that a mesoporous silica thin film (270 nm) is capable of replacing the conventional polymer based membranes with an improvement in the power generated over conventional direct glucose fuel cells.

## 1. Introduction

Cardiovascular disease (CVD) remains the greatest cause of mortality in the USA and worldwide.[1] Consequently, there is an upsurge in the various novel implantable devices to diagnose, monitor, and treat cardiovascular disease.[2–6] Since most of these implantable devices need to operate for long time durations, the research focus has shifted towards the development of compact, efficient and low-power consuming implants. With the emergence of micro-electro mechanical system (MEMS) based implantable devices, fabrication of low-power devices can now be realized.[7–17] But for even very low-power consuming devices, use of batteries is not considered to be a viable long-term solution due to their very limited life-span (Table S1, ESI†), while the life-span of the patient may be more than 20 years, resulting in unnecessary pain and cost to the patient. Further, there is a desire to integrate newer devices such as heart failure warning systems, glucose and electrolyte sensors with systems such as an automated implantable cardioverter defibrillator (AICD) and pacemakers. Implantable direct glucose fuel cells (biofuel cells) provide an alternative continuous power source to recharge batteries and are capable of oxidizing glucose to generate electricity.[18] The only byproducts of the electrochemical reactions are benign substances including water and gluconic acid or carbon dioxide.[19] A common problem with direct glucose fuel cells is the lack of an inorganic catalyst that can selectively oxidize glucose from blood. The presence of oxygen in blood interferes with glucose oxidation at the anode. Hence there has been significant effort to develop anodic materials for the sandwiched-electrode design (Fig. S1, ESI†), which reduces oxygen at the oxygen-selective cathode, leaving glucose for oxidation at the anode. Little research has been focused to date on the membrane itself, however. Weakly ionic polymer membranes such as polyvinyl alcohol–polyacrylic acid cross-linked hydrogels, sulfonated polypropylene and cuprophan,[20–22] have been used to facilitate glucose diffusion and separate the electrodes. Rao *et al.*[20,23] and Atanasov and Wilkins[24] have used hydrophobic membranes to attract oxygen molecules. Since oxygen dissolves rapidly in hydrophobic membranes, hydrophilic membranes are used to minimize oxygen crossover to the anode.[20,21,25] A common deficiency with all polymer membranes is the random polymerization, which leads to high variation in the physical properties (pore sizes, pore distribution, and porosity) of the membrane. Further, the thickness of the membranes is typically on the order of a few hundred microns,

[a]*Department of Biomedical Engineering, University of Texas at Austin, Austin, TX, 78712, USA. E-mail: john.zhang@engr.utexas.edu*
[b]*Nanomedicine and Biomedical Engineering, The Methodist Hospital Research Institute, Houston, TX, USA*
[c]*Mechanical Engineering and the Materials Science and Engineering Program, University of Texas at Austin, Austin, TX, USA*
[d]*University of Texas Health Science Center at San Antonio, San Antonio, TX, USA*
[e]*South Texas Veterans Administration Health Care System, San Antonio, TX, USA*
† Electronic supplementary information (ESI) available. See DOI: 10.1039/c1lc20119k
‡ Equal contributing authors.

increasing the overall direct glucose fuel cell thickness and presenting a significant diffusion barrier for glucose. Moreover, polymer membrane are prone to swell, delaminate, and have been a locus for infection when implanted *in vivo*.[20,23] These problems can be circumvented by using inorganic mesoporous (nanoporous) silica (MPS) membranes. MPS has been used previously as molecular sieves, in high surface area catalysis, and for drug delivery and opto-electronic devices.[26–32]

Our present focus is on strategies that can enable creation of high-power direct glucose fuel cells. This can be achieved by shifting the implant site from a sub-clavicular skin pouch to an intra-venous stent mounted implant. Moving the implant site helps by increasing glucose diffusion rates. It is estimated that the glucose mass-transfer rate in the case of intra-venous implants is enhanced by blood flow of 1–10 cm $s^{-1}$, and is expected to be 1–2 mA $cm^{-2}$.[33] Whereas the same implant in tissues in the absence of convection would account for glucose flux rates limited to only 0.2 mA $cm^{-2}$.[20] However, reduction in the thickness of the present fuel cell is critical for a stent based application. Hence the motivation behind the use of ultra-thin MPS as the membrane is two-fold: (1) to provide well controlled physico-chemical properties of the nanopores (shape, size, distribution, and surface functionalization) for enhanced glucose diffusion; and (2) to drastically reduce the thickness of the direct glucose fuel cell. Since the problem associated with the use of blood glucose is diffusion in sufficient concentration, reduction in the membrane thickness would also help boost the efficiency of the direct glucose fuel cell by reducing the path-length of the glucose molecules.[34] Combining the above mentioned strategies, we have assembled a highly efficient, ultra-thin direct glucose fuel cell.

## 2. Experimental

### 2.1. Electrode fabrication

The *anode* was made of platinum thin-film (thickness: 25 nm), e-beam evaporated on a commercial silicon wafer (500 μm, $\rho < 0.05$ Ω cm, P-type). The silicon wafers were then diced into 5 × 5 $mm^2$ anodes. Contact angles of the anode surface were measured by a goniometer with captive bubble contact angle measurement. The *cathode* was constructed of chemically reduced graphene oxide as reported elsewhere.[35] Graphite oxide was obtained using the modified Hummers method. The agglomerates of reduced graphene oxide platelets were assembled into electrodes by mixing with 5% polytetrafluoroethylene (PTFE) binder and rolled into 65 μm thick sheets. Activated carbon (Norit Super 30) was used as the control for comparison with the reduced graphene oxide based electrodes and 5% PTFE was also used as the binder for the activated carbon. The thickness of the activated carbon sheets was 210 μm. Fabricated carbon sheets were then manually pressed on the stainless steel mesh (wire diameter: 0.12 mm, square size: 0.72 mm, percentage of open area: 73%) to obtain cathodes. Comparison of all the electrode thicknesses along with their performance has been included in Table S2, ESI†. The electrodes were soaked in phosphate buffered saline (PBS, pH 7.4) solution overnight, prior to use in direct glucose fuel cell assemblies. When not in use, the electrodes were stored in PBS under anaerobic atmosphere.

### 2.2. Preparation and characterizations of mesoporous silica thin film on anodes

Most of the procedures used for the synthesis of MPS have been described elsewhere[27] and are summarized in Fig. S2, ESI†. Briefly, 14 ml of tetraethyl orthosilicate (TEOS) was dissolved in a mixture of 15 ml of ethanol, 6.5 ml of distilled water, and 0.3 ml of 6 M HCl and stirred for 2 h at 75 °C to form a clear silicate sol. Separately, 1.2 g of Pluronic L64 was dissolved in 30 ml of ethanol by stirring at room temperature. The coating solution was prepared by mixing 10 ml of the silicate sol into the triblock co-polymer solution followed by stirring of the resulting sol–gel for 2 h at room temperature. The pH of the mixture solution remained around 1.5. The coating sol was deposited on a platinum coated silicon (100) wafer by spin-coating at a spin rate of 2000 rpm for 20 s. To increase the degree of polymerization of the silica framework in the films and to further improve their thermal stability, the as-deposited films were heated at 80 °C for 12 h. The films were calcinated at 425 °C to remove the organic surfactant. The temperature was raised at a heating rate of 1 °C $min^{-1}$, and the furnace was heated at 425 °C for 5 h. Oxygen plasma ashing was performed in a plasma asher (March Plasma System) to pre-treat the chip surface. The treatment was carried out with an $O_2$ flow rate at 80 sccm and a power of 300 W for 10 min. The fabricated MPS coated anodes were diced into 5 × 5 $mm^2$ or 5 × 10 $mm^2$ sizes for *in vitro* and *in vivo* experiments, respectively. The characterization of nanotexture on MPS chips was carried out by transmission electron microscopy (TEM), $N_2$ adsorption/desorption analysis, ellipsometry and small angle X-ray diffraction (XRD).

### 2.3. Assembly of *in vitro* direct glucose fuel cells

Three different types of direct glucose fuel cell with a Pt anode were assembled in the present study: (1) the cell with activated carbon as cathode and surfactant coated polypropylene as membrane, labeled Pt/PP/AC, (2) the cell with reduced graphene oxide as cathode and surfactant coated polypropylene as membrane, labeled Pt/PP/G and (3) the cell with reduced graphene oxide as cathode and MPS as membrane, labeled Pt/MPS/G.

Fig. 1a and b show the schematic of the direct glucose fuel cells assembled. For the polymer membrane based direct glucose fuel cell, surfactant-coated polypropylene membranes (25 μm, average pore size: 64 nm, Celgard 3501) were placed between the electrodes. The porous membrane acted as the insulator while simultaneously providing glucose diffusion across the membrane. Since the anode is comprised of conductive silicon, which is non-catalytic in nature,[36] the stainless steel mesh based current collector (160 μm) was placed directly beneath the Pt/Si anode. The electrodes were stacked as shown in Fig. 1a and b. Polydimethylsiloxane (PDMS) sheets with thickness (1–2 mm) provided mechanical support to the silicon anodes while damping the pressure on the anode due to the clamp.

The packaged direct glucose fuel cell is shown in Fig. 1c. Except for the contact portion of the current collector, the remaining current collector was covered either with two-part epoxy or hot glue. The epoxy coated current collector was cured at 80 °C for 20 min. The epoxy coated direct glucose fuel cell was placed inside a glass beaker containing 0.1% glucose solution (5 mM) dissolved in PBS (pH 7.4). Any air that was trapped

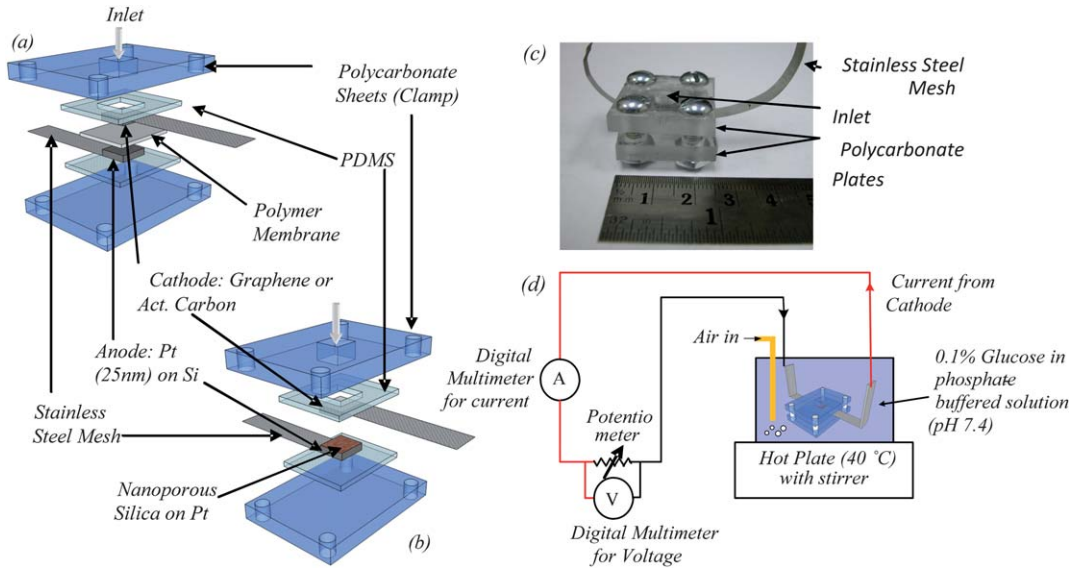


**Fig. 1** Schematic for direct glucose fuel cells using (a) polymer membrane, and (b) mesoporous silica as the membrane. (c) Packaged direct glucose fuel cell before covering the stainless steel mesh with epoxy. (d) Experimental setup schematic for direct glucose fuel cell load characterizations.

during assembly was removed by placing the glass beaker containing the direct glucose fuel cell in glucose solution under vacuum for 15 min. The setup was then placed on a hot plate at 40 °C with continuous stirring to simulate physiological conditions. Throughout the experiments, the solution was continuously aerated. To measure the load characteristics of the assembled direct glucose fuel cell, the terminals were connected to a variable external resistance (0–12 kΩ), as shown in Fig. 1d. Multiple datasets were acquired and averaged for the same set of parameters. Averaged values were re-plotted as the power density and polarization curves.

### 2.4. Assembly and implantation of the *in vivo* direct glucose fuel cell

For *in vivo* experiments, the 10 × 5 $mm^2$ MP silica coated anodes were used to assemble the direct glucose fuel cell. Reduced graphene oxide pressed on stainless steel mesh was used as the cathode. The two electrodes were carefully pressed between two polycarbonate sheets (13 × 5 × 1 $mm^3$). Polycarbonate sheets were locked in place using stainless steel screws. The stainless steel mesh protruding from the direct glucose fuel cell was twisted into a wire-shape and covered using thermoplastic glue. Alligator clips were used to connect the tip of rolled stainless steel mesh to the external load (as described above). Assembled direct glucose fuel cells were placed in glucose-free PBS solution and vacuumed for 15 min. Direct glucose fuel cells were then stored in PBS till the actual implantation.

For implantation inside the heart, a purse-string suture was tied to the anterior wall of the right ventricle in a Yorkshire pig. An incision was made directly through the right ventricular myocardium. The direct glucose fuel cell was inserted into the right ventricular chamber and the purse-string closed to maintain hemostasis. All porcine studies were performed with approval of Institutional Animal Care and Use Committee (IACUC) at the University of Texas Health Science Center in San Antonio.

## 3. Results

### 3.1. Mesoporous silica

Using a spectroscopic ellipsometer, the thin film MPS thickness and porosity were measured to be 281.8 ± 7.5 nm and 44.8 ± 0.13%, respectively. In Fig. 2a, the TEM image of the plan view of the mesoporous silica thin film depicts a worm-like nanostructure throughout the porous layer. In Fig. 2b $N_2$ adsorption/desorption curves were generated using a Quantachrome Autosorb-3b BET Surface Analyzer (inset) and the pore size distribution (3.2 nm) was calculated using the Barrett–Joyner–Halenda (BJH) method. The adsorption/desorption isotherms describe a Type IV isotherm with a $H_2$ hysteresis loop (sloping adsorption branch and nearly vertical desorption branch), indicating a mesoporous silica structure with interconnecting channels. Inflection points appearing at $0.40 < P/P_0 < 0.75$ indicated the formation of "ink-bottle" shaped nanopores. TEM images and ellipsometry results did not show any changes in the structure or thickness of the MPS, demonstrating it was durable for standard sterilization procedures (data not shown). It was also

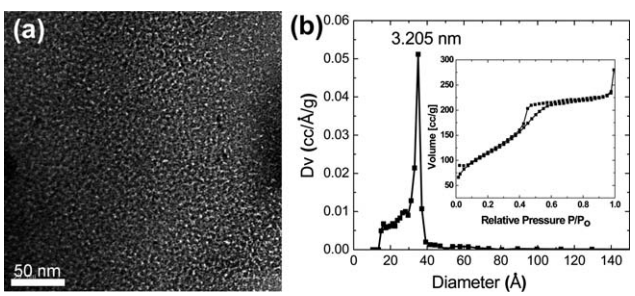


**Fig. 2** The characterization of mesoporous silica thin films prepared using Pluronic L64. (a) TEM image of plan-view of MPS thin film. (b) $N_2$ adsorption/desorption analysis (pore size distribution and isotherms in the insets).

found that MPS retained its hydrophilic surface whereas the polypropylene membrane turned hydrophobic (Fig. S3 and Table S3, ESI†)

### 3.2. Direct glucose fuel cell performance

The fuel cell showed negligible open circuit potential in PBS and the potential rapidly rises when glucose was added to the solution (data not shown).

**A. Performance in 0.1% (5 mM) glucose.** A Pt/MPS/G direct glucose fuel cell (5.3 μW $cm^{-2}$) shows higher power density compared to a Pt/PP/G direct glucose fuel cell (2.1 μW $cm^{-2}$) indicating better performance of the direct glucose fuel cell when the polypropylene membrane was replaced with mesoporous silica membrane. Fig. 3 shows the comparison of the power densities and polarization values obtained from the various direct glucose fuel cells assembled. Normalizing the current densities of Fig. 3a and b to the glucose concentration gradient (Table S4, Section S1, and Fig. S4, ESI†) eliminates the variation in the performance due to membrane thickness differences.

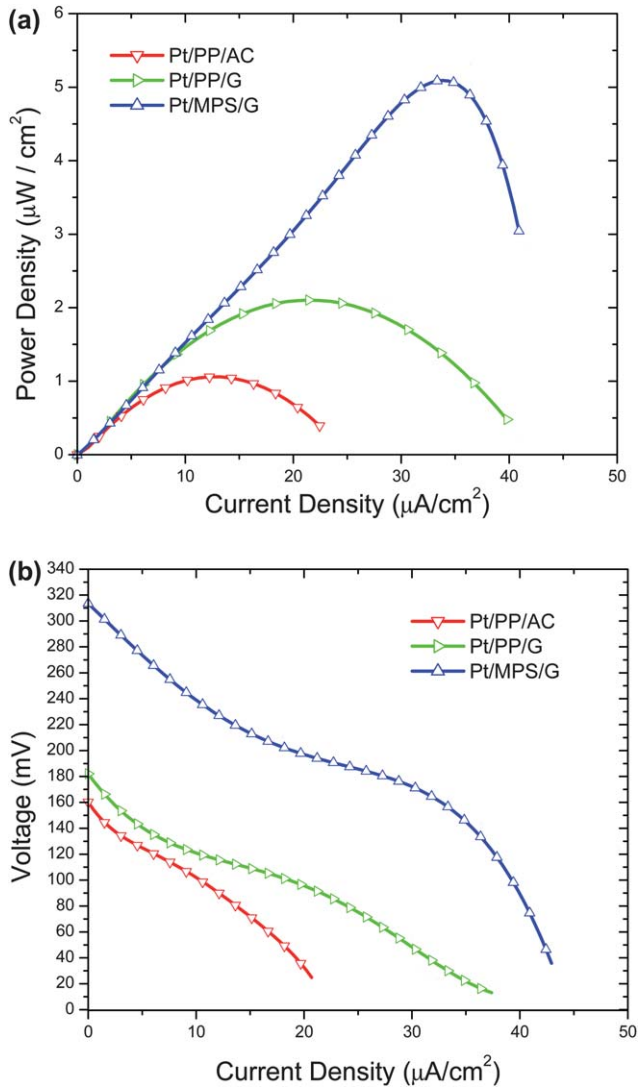


**Fig. 3** Experimental results obtained with mesoporous silica *vs.* polypropylene membrane based direct glucose fuel cells: (a) power density curves and (b) polarization curves. Standard deviations were below 5%.

Kerzenmacher *et al.*[37] have reported previously that the presence of oxygen has a greater impact on the anode open circuit potential than on the polarization curve for anodes subjected to the same electrolyte conditions. Pt/MPS/G shows significantly higher open circuit potential (314.6 mV) compared to Pt/PP/G (181.4 mV) and Pt/PP/AC (160.0 mV). Reduced graphene oxide as a cathode shows an increase in performance (2.1 μW $cm^{-2}$) compared to a similar setup based on activated carbon (1.1 μW $cm^{-2}$) in the present study.

**B. Comparison with performance in 0.42% glucose (22 mM).** All the direct glucose fuel cells assembled in the present study showed reduced power density values compared to our previous study.[38] This was due to the lower glucose concentration used in the present study (0.1%) which is more consistent with physiological glucose concentration. The presence of oxygen also had an effect on the open circuit potential of the direct glucose fuel cells, which was lower for cells in 0.1% glucose solution. Values of interest have been summarized in Table S2, ESI†.

**C. Comparison with the literature.** The power densities reported in the present study obtained from activated carbon (1.1 μW $cm^{-2}$) based fuel cell are lower compared to the earlier literature by Kerzenmacher *et al.* (1.4 μW $cm^{-2}$, Table S2, ESI†) while the open circuit potentials obtained in the present study are significantly lower.[21] This indicates leakage of oxygen to the anodic side which could be due to the reduced thickness of the activated carbon cathode (200 μm) used in the present study compared to the literature (thickness of 400–800 μm).[19,21] Carbon based cathodes help remove the oxygen from the incoming mixture of glucose and oxygen. Hence optimal cathode thickness is necessary to ensure an anaerobic environment at the anode. Thus, reduction in the membrane thickness can play a pivotal role in the overall reduction of the direct glucose fuel cell thickness without compromising performance.

**D. Performance of *in vivo* direct glucose fuel cells.** The value of the Pt/MPS/G was further demonstrated during the *in vivo* experiments. Fig. 4b shows the performance of the device when implanted into venous blood of a live pig. In comparison, the same device had improved performance *in vivo* (10 μW $cm^{-2}$, Fig. 4) than during *in vitro* experiments (6 μW $cm^{-2}$, Table S2, ESI†) due to six times lower oxygen concentration and higher flow rates in venous blood. The total time of the study was 12 min before the pig died. In another porcine experiment, which was performed for over 50 min, deposition of blood clots and fibrinogenic coating was noticed on the surface of the device (Fig. 4a). However, the device continued to deliver constant power output (on external load of 10 kΩ, $i = 20.3$ μA) over the period of 50 min.

## 4. Discussions

Several studies have focused on the development of enzymatic direct glucose fuel cells using immobilized enzymes for anodes and/or cathodes, and clinically significant power densities have

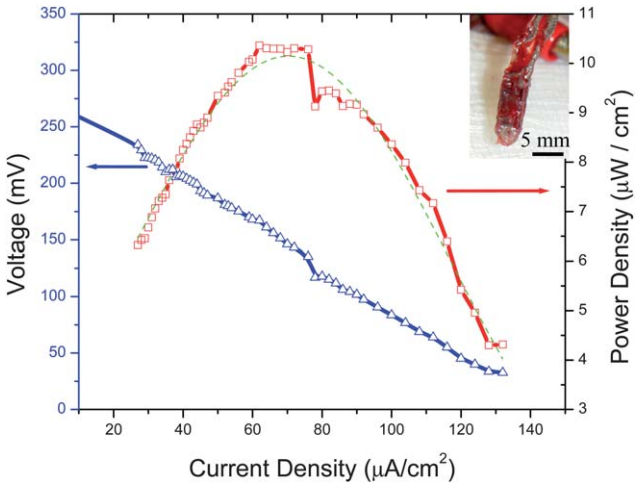


**Fig. 4** *In vivo* performance: plot for *in vivo* studies showing high power density obtained from a direct glucose fuel cell implanted in the right-ventricle of a live Yorkshire pig; inset: photograph of the device after removal from the porcine right ventricle following 50 min of implantation showing device size (front view) and fibrinogenic deposition.

been reported from such systems.[39–44] However, there are numerous problems associated with the use of enzyme based direct glucose fuel cells. Effective transport of electrons from the site of catalysis to the electrode surface, durability of enzymes under physiological conditions, operational pH ranges, biocompatibility of enzymes, electron mediators, and sterilization challenges still remain largely unaddressed.[45–47] The direct glucose fuel cell reported in this study presents an attractive alternative to enzymatic biofuel cells in terms of sterility, biocompatibility, stability and performance. The use of inorganic materials in the construction of the current direct glucose fuel cell removes the problem of sterilization. The autoclaving results corroborate this finding. Although the biocompatibility of the reduced graphene oxide used here has not yet been proven, 'paper' comprised of stacked and overlapped reduced graphene oxide platelets has been documented to be biocompatible.[48] Mesoporous silica membrane is made from silicon, oxygen and hydrogen atoms arranged in a crystal lattice. The atoms are held together by covalent bonds. Hence there is no permeation of water molecules between layers. In polymer based membranes, water seeps into gaps between the layers, however. This seepage of water causes swelling. Inorganic membranes have been extensively shown to be resistant to swelling previously.[49,50] Hence, with the use of mesoporous silica, we have also addressed the problem of swelling and infections commonly encountered with polymeric membranes used in direct glucose fuel cells.

Previous studies have shown that activated carbon is selective towards oxygen reduction only.[19,20,23,51] Glucose reduction does not take place on the cathode in principle. This is the major reason for choosing activated carbon as the cathode over other possible materials. In the present study, we have demonstrated the use of reduced graphene oxide as an alternative cathodic material to the conventionally used activated carbon. It has been proposed that oxygen reduction in activated carbon occurs at the edges of the layers that make up the structure of activated carbon whereas the micropores may not be used for oxygen reduction.[52] Reduced graphene oxide based cathodes used in the present study contain several reduced graphene oxide layers bound together using PTFE (polytetrafluoroethylene). Activated carbon based cathodes, on the other hand, contain several amorphous activated carbon granules bound using PTFE. Hence, only a fraction of the whole activated carbon granule surface would be chemically active. Concentration gradient-normalized plots (Fig. S4, ESI†) were found to be in corroboration with the above claims. Further rigorous studies need to be performed to evaluate the efficacy of reduced graphene oxide as a cathodic material for implantable biofuel cells.

Normalized plots (Fig. S4, ESI†) indicated that the enhanced power density was due to the hydrophilic nature of the mesoporous silica membrane. Contact angle measurements showed that the surfactant-coated polypropylene membrane was hydrophobic in nature. This could have been due to degradation of the surfactant coating, which makes the surface hydrophilic for rapid wetting. However, mesoporous silica shows stable surface chemistry and has a long shelf life,[53] making it ideal for direct glucose fuel cell application. The power performance of the presented direct glucose fuel cells was considerably higher than other literature values (Table S2, ESI†) indicating the contribution of reduced graphene oxide and hydrophilic mesoporous silica towards increasing the power output. In the presence of oxygen along with glucose, oxygen gets preferably adsorbed on the platinum surface.[19] This leads to an increase in the anode potential thereby causing a drop in the open circuit potential (Section S2, ESI†) of the direct glucose fuel cell. The higher open circuit potential of Pt/MPS/G (314.6 mV) compared to Pt/PP/G (181.4 mV) indicates that there is lower crossing of oxygen to the anode, which can be attributed to the hydrophilic nature of the mesoporous silica membrane.

Moreover, the direct glucose fuel cells tested here were investigated under 21% oxygen saturation conditions. However, in blood oxygen saturation levels of 5%, even higher power densities can be anticipated from the same direct glucose fuel cells. An example of this would be the *in vivo* porcine performance of the Pt/MPS/G direct glucose fuel cell which demonstrated power density as high as 10 $\mu W\ cm^{-2}$. This is the highest power density obtained to date for a direct glucose fuel cell based on inorganic metal catalysts. With such a high power density output, the lifetime of a pacemaker (Table S1, ESI†) could be extended from 7 years to 12 years. However, longer duration experiments need to be performed to confirm the continuous performance of the direct glucose fuel cell over time. Other studies have shown functional capability of a direct glucose fuel cell *in vitro* for 235 days and *in vivo* up to 150 days.[19,20] However, there are no reports of chronic implanted direct glucose fuel cell in blood vessels to date. It is anticipated that devices implanted in veins will be subject to lower oxygen concentrations, but pose greater barriers to glucose diffusion with neo-intimal tissue formation at the same time. Thus it will be critical to evaluate the chronic performance of an intra-vascular implanted direct glucose fuel cell in the future.

## 5. Conclusions

Use of advanced nanomaterials makes it possible to fabricate an ultra-thin direct glucose fuel cell capable of delivering high power densities, which was not feasible for earlier direct glucose fuel cell designs. We presented preliminary results on the use of mesoporous

 

silica as a functional membrane and reduced graphene oxide as the cathode for the fabrication of ultra-thin implantable direct glucose fuel cells. Load characteristics were measured for the assembled direct glucose fuel cells and showed the potential of using mesoporous silica as a membrane for direct glucose fuel cells. Further research is needed to establish the significant advantages of using mesoporous silica along with its optimization. As mesoporous silica and graphene processing are becoming semiconductor clean-room friendly, the future holds great promise for the development of mass-producible, high power-density, ultra-thin direct glucose fuel cells for biomedical implant applications.

## Acknowledgements

This research was performed at the Biomedical Engineering Department, the Mechanical Engineering Department and the Microelectronics Research Center (MRC) at UT Austin, a member of the National Nanofabrication Infrastructure Network (NNIN). We are grateful to The University of Texas at Austin for a Special Research Grant (SRG) to partly support this research. The authors at the Department of Nanomedicine and Biomedical Engineering (nBME) acknowledge the grant support from the following agencies: NASA (NNJ06HE06A) and the State of Texas Emerging Technology Fund. We thank Dr Sanjay Banerjee for providing the platinum electrode materials. MS and RSR appreciate support (startup funds) from The University of Texas at Austin. We also thank Drs Porterfield and Hacker, and Danny Escobedo for the invaluable help with the *in vivo* porcine studies. We are also grateful to the Veterans Administration (VA) Merit Grant for the support with porcine studies.

## References

1 M. Writing Group, D. Lloyd-Jones, R. Adams, M. Carnethon, G. De Simone, T. B. Ferguson, K. Flegal, E. Ford, K. Furie, A. Go, K. Greenlund, N. Haase, S. Hailpern, M. Ho, V. Howard, B. Kissela, S. Kittner, D. Lackland, L. Lisabeth, A. Marelli, M. McDermott, J. Meigs, D. Mozaffarian, G. Nichol, C. O'Donnell, V. Roger, W. Rosamond, R. Sacco, P. Sorlie, R. Stafford, J. Steinberger, T. Thom, S. Wasserthiel-Smoller, N. Wong, J. Wylie-Rosett, Y. Hong and C. for the American Heart Association Statistics and S. Stroke Statistics, *Circulation*, 2009, **119**, e21–e181.
2 B. Huegl, H.-J. Bruns, C. Unterberg-Buchwald, A. Grosse, B. Stegemann, B. Lauer, J. C. Geller and M. Gasparini, *J. Cardiovasc. Electrophysiol.*, 2006, **17**, 813–817.
3 *US Pat*. 5609615, 1997.
4 *US Pat*. 5423883, 1995.
5 *US Pat*. 5609614, 1997.
6 G. S. Kassab, M. Svendsen, W. Combs, J. S. Choy, E. J. Berbari and J. A. Navia, *Am. J. Physiol. Heart Circ. Physiol.*, 2010, **298**, H287–H293.
7 D. J. Laser and J. G. Santiago, *J. Micromech. Microeng.*, 2004, **14**, R35.
8 A. T. Evans, J. M. Park, S. Chiravuri and Y. B. Gianchandani, *Biomed. Microdevices*, 2010, 12, 159–168.
9 M. Tijero, G. Gabriel, J. Caro, A. Altuna, R. Hernandez, R. Villa, J. Berganzo, F. J. Blanco, R. Salido and L. J. Fernandez, *Biosens. Bioelectron.*, 2009, **24**, 2410–2416.
10 P. G. Silveira, C. W. T. Miller, R. F. Mendes and G. N. Galego, *Clinics*, 2008, **63**, 59–66.
11 S. Reichelt, J. Fiala, A. Werber, K. Forster, C. Heilmann, R. Klemm and H. Zappe, *IEEE Trans. Biomed. Eng.*, 2008, **55**, 581–588.
12 R. Schlierf, U. Horst, M. Ruhl, T. Schmitz-Rode, W. Mokwa and U. Schnakenberg, *J. Micromech. Microeng.*, 2007, **17**, S98–S102.
13 P. Cong, D. J. Young and W. H. Ko, in *Proceedings of the IEEE Sensors 2004*, ed. D. Rocha, P. M. Sarro and M. J. Vellekoop, IEEE, New York, 2004, vol. 1–3, pp. 1359–1362.
14 R. Arzbaecher, Z. Song, M. Burke and J. Jenkins, *Circulation*, 2004, **110**, 1097–1097.
15 B. Kjellstrom, C. Linde, T. Bennetta, A. Ohlsson and L. Ryden, *Eur. J. Heart Failure*, 2004, **6**, 627–634.
16 H. L. Chau and K. D. Wise, *IEEE Trans. Electron Devices*, 1988, **35**, 2355–2362.
17 N. Najafi and A. Ludomirsky, *Biomed. Microdevices*, 2004, **6**, 61–65.
18 S. K. Wolfson, Jr, S. L. Gofberg, P. Prusiner and L. Nanis, *Trans. - Am. Soc. Artif. Intern. Organs*, 1968, **14**, 198–203.
19 S. Kerzenmacher, J. Ducree, R. Zengerle and F. von Stetten, *J. Power Sources*, 2008, **182**, 1–17.
20 E. Weidlich, G. Richter, F. Vonsturm, J. R. Rao, A. Thoren and H. Lagergren, *Biomater., Med. Devices, Artif. Organs*, 1976, **4**, 277–306.
21 S. Kerzenmacher, J. Ducree, R. Zengerle and F. von Stetten, *J. Power Sources*, 2008, **182**, 66–75.
22 J. R. Rao, G. J. Richter, F. Vonsturm and E. Weidlich, *Bioelectrochem. Bioenerg.*, 1976, **3**, 139–150.
23 J. R. Rao and G. Richter, *Naturwissenschaften*, 1974, **61**, 200–206.
24 P. Atanasov and E. Wilkins, *Biotechnol. Bioeng.*, 1994, **43**, 262–266.
25 J. R. Rao, G. Richter, S. F. Von and E. Weidlich, *Ber. Bunsenges. Phys. Chem.*, 1973, **77**, 787–790.
26 A. Bouamrani, Y. Hu, E. Tasciotti, L. Li, C. Chiappini, X. Liu and M. Ferrari, *Proteomics*, 2009, **10**, 496–505.
27 M. Ferrari, *Nat. Rev. Cancer*, 2005, **5**, 161–171.
28 M. C. Ferrari, S. Carranza, R. T. Bonnecaze, K. K. Tung, B. D. Freeman and D. R. Paul, *J. Membr. Sci.*, 2009, **329**, 183–192.
29 Y. Hu, A. Bouamrani, E. Tasciotti, L. Li, X. Liu and M. Ferrari, *ACS Nano*, 2010, **4**, 439–451.
30 Y. Hu, D. H. Fine, E. Tasciotti, A. Bouamrani and M. Ferrari, Nanodevices in diagnostics, *Wiley Interdiscip. Rev.: Nanomed. Nanobiotechnol.*, 2011, **3**(1), 11–32.
31 Y. Bai, H. Yang, W. Yang, Y. Li and C. Sun, *Sens. Actuators, B*, 2007, **124**, 179–186.
32 C. Ispas, I. Sokolov and S. Andreescu, *Anal. Bioanal. Chem.*, 2009, **393**, 543–554.
33 S. C. Barton and P. Atanassov, *Abstr. Pap. Am. Chem. Soc.*, 2004, **228**, 004-FUEL.
34 M. Beltzer, J. S. Batzold, *Limitations of Blood Plasma as a Fuel Cell Electrolyte*, 1969.
35 M. D. Stoller, S. J. Park, Y. W. Zhu, J. H. An and R. S. Ruoff, *Nano Lett.*, 2008, **8**, 3498–3502.
36 Y. K. Choi, G. Wang, M. H. Nayfeh and S. T. Yau, *Biosens. Bioelectron.*, 2009, **24**, 3103–3107.
37 B. B. A. Kloke, S. Kerzenmacher, U. Kräling, R. Zengerle and F. von Stetten, *A Single Layer Biofuel Cell as Potential Coating for Implantable Low Power Devices*, 2008.
38 T. Sharma, Y. Hu, A. Gopal, M. Stoller, K. Lin, R. S. Ruoff, M. Ferrari and X. J. Zhang, presented in part at the Power MEMS 2009, Washington DC, December 1–4, 2009.
39 T. Chen, S. C. Barton, G. Binyamin, Z. Q. Gao, Y. C. Zhang, H. H. Kim and A. Heller, *J. Am. Chem. Soc.*, 2001, **123**, 8630–8631.
40 A. Heller, *Anal. Bioanal. Chem.*, 2006, **385**, 469–473.
41 A. Heller, *Phys. Chem. Chem. Phys.*, 2004, **6**, 209–216.
42 H. H. Kim, N. Mano, X. C. Zhang and A. Heller, *J. Electrochem. Soc.*, 2003, **150**, A209–A213.
43 N. Mano, F. Mao, W. Shin, T. Chen and A. Heller, *Chem. Commun.*, 2003, 518–519.
44 N. Mano, V. Soukharev and A. Heller, *J. Phys. Chem. B*, 2006, **110**, 11180–11187.
45 C. Kang, H. Shin and A. Heller, *Bioelectrochemistry*, 2006, **68**, 22–26.
46 F. Mao, N. Mano and A. Heller, *J. Am. Chem. Soc.*, 2003, **125**, 4951–4957.
47 Z. W. Zhu, C. Momeu, M. Zakhartsev and U. Schwaneberg, *Biosens. Bioelectron.*, 2006, **21**, 2046–2051.
48 H. Chen, M. B. Muller, K. J. Gilmore, G. G. Wallace and D. Li, *Adv. Mater.*, 2008, **20**, 3557–3561.
49 K. L. Chu, S. Gold, V. Subramanian, C. Lu, M. A. Shannon and R. I. Masel, *J. Microelectromech. Syst.*, 2006, **15**, 671–677.
50 K. L. Chu, M. A. Shannon and R. I. Masel, *J. Micromech. Microeng.*, 2007, **17**, S243–S249.
51 P. J. Sharrock, J. M. Courtney, T. Gilchrist and S. Affrossman, *Anal. Lett.*, 1976, **9**, 1085–1090.
52 D. Qu, *Carbon*, 2007, **45**, 1296–1301.
53 S. Kaufhold, R. Dohrmann and C. Ulrichs, *Appl. Clay Sci.*, 2008, **41**, 158–164.